# Managing $H_2O$ Cross-Sensitivity Using Composite Electrolyte $NO_x$ Sensors

Erica Perry Murray, Khawlah Kharashi and
Kehinde Adedeji

**Abstract**

$NO_x$ sensors composed of partially stabilized zirconia (PSZ), fully stabilized zirconia (FSZ), and PSZ–FSZ composite electrolytes were investigated using impedance spectroscopy under dry and humidified gas conditions. The impedance data were used to interpret the electrochemical behavior of the various sensors as the water concentration in the gas stream varied. The sensors were operated in the presence of 0–100 ppm NO with 1–18% $O_2$ and 3–10% $H_2O$ with $N_2$ as the balance gas. The operating temperature of the sensors ranged from 600 to 700°C. The impedance response for sensors containing ≥ 50 vol% PSZ slightly decreased under humidified gas conditions, in comparison to dry gas conditions; whereas, a significant increase in impedance occurred for sensor largely containing FSZ. This indicated water cross-sensitivity was substantial at FSZ-based sensors. The microstructural properties, $NO_x$ sensitivity, oxygen partial pressure and temperature dependence, as well as the response time of the sensors composed of the various electrolytes were characterized in order to interpret the electrochemical response with respect to water cross-sensitivity. Analysis of the data indicated that sensors composed of a PSZ–FSZ composite electrolyte with 50 vol% PSZ were more suitable for detecting $NO_x$ while limiting water cross-sensitivity.

**Keywords:** $NO_x$ sensors, porous zirconia, impedancemetric gas sensing, partially stabilized zirconia, YSZ

## 1. Introduction

Advancements in diesel engine technology and emissions regulations in various countries are driving the need for $NO_x$ sensors capable of greater sensitivity, selectivity, and accuracy. Zirconia-based $NO_x$ sensors are favored for their stability and electrochemical performance under stringent

exhaust conditions. Various research studies have achieved substantial $NO_x$ sensitivity at sensors utilizing novel porous electrolytes, as an alternative to the conventional dense electrolyte microstructure [1–3]. $NO_x$ sensors based on the conventional architecture commonly have porous precious metal electrodes to support exhaust gas transport to the electrode/electrolyte interface where $NO_x$ sensing reactions take place. Unfortunately, heterogeneous catalysis can occur within the porous electrodes, thereby reducing the amount of $NO_x$ gas arriving at the interface. This becomes a significant problem when it is necessary to detect low concentrations (i.e., <10 ppm) of $NO_x$ as sensor accuracy is compromised. Heterogeneous catalysis is negligible at $NO_x$ sensors using a porous zirconia-based electrolyte with dense electrodes. The porous electrolyte does not appear to interfere with the exhaust gas during transport to the electrode/electrolyte interface. Thus, the porous zirconia electrolyte enables greater $NO_x$ sensor sensitivity and accuracy. However, cross-sensitivity to interfering exhaust gases, particularly water vapor, adversely affects the selectivity of the device. Sensor operation at specific frequencies appears to be an effective measure for addressing cross-sensitivity to oxygen [1]. Yet, this approach has not been effective for limiting cross-sensitivity to water. Greater understanding of the behavior of water during sensor operation is necessary for managing water cross-sensitivity and improving the feasibility of porous zirconia-based $NO_x$ sensors.

Cross-sensitivity in $NO_x$ sensors can result from electrochemical reactions with exhaust gas species that proceed more readily and/or more rapidly than $NO_x$ reactions. Accumulation of various molecules at the electrode/electrolyte interface can also enable undesirable reactions to proceed leading to cross-sensitivity. The impact of water cross-sensitivity has been ambiguous as it can cause the $NO_x$ sensing response to increase or decrease [4–6]. Some studies suggest that the different behavior observed is related to the sensor materials, fabrication methods, and operating conditions. Few studies have reported the $NO_x$ sensing response for various water concentrations. Limited data with varying results has made it difficult to understand and control the impact of water on the sensing behavior of porous electrolyte $NO_x$ sensors.

Recently, the authors found composite electrolyte $NO_x$ sensors with a porous microstructure demonstrated reduced cross-sensitivity to water, in comparison to sensors with a single-phase electrolyte. To further study the potential of composite electrolytes for $NO_x$ sensing, various sensors based on electrolytes containing specific ratios of partially stabilized zirconia (PSZ) and fully stabilized zirconia (FSZ) were evaluated using the impedancemetric technique. The work presented in this chapter describes the electrochemical response, gas sensitivity, rate limiting mechanisms, and sensing response rate due to operation in humidified gas environments for composite electrolyte $NO_x$ sensors.

## 2. Experimental

Standard ceramic processing techniques were used to fabricate $NO_x$ sensors containing partially-stabilized zirconia (PSZ, 4.7 mol% $Y_2O_3$–$ZrO_2$) produced by advanced ceramics and fully stabilized zirconia (FSZ, 8 mol% $Y_2O_3$–$ZrO_2$) manufactured by Tosoh as electrolyte

materials. There were five electrolyte slurries prepared using different ratios of PSZ and FSZ along with polyvinyl butyral (Butvar B-76) binder and ethanol for the solvent. The slurries were ball milled for 16 hours to form a uniform mixture. A portion of each electrolyte slurry was dried and the powders were pressed uniaxially at 200 MPa into pellets. The three types of PSZ–FSZ composite electrolytes studied contained 25, 50, and 75 vol% PSZ, and are identified as 25 PSZ–75 FSZ, 50 PSZ–50 FSZ, and 75 PSZ–25 FSZ, respectively. Electrolytes composed of single-phase FSZ or single-phase PSZ particles were fabricated for performance comparison purposes. Single-phase PSZ electrolytes containing coarse particles were also fabricated in order to study the impact of particle size on water cross-sensitivity. Gold (Au) electrodes were placed over the electrolytes and coated using the corresponding electrolyte slurry to complete the sensor configuration. The sensors were air dried and then fired at 1050°C for a period of 1 hour. A schematic of the top view and cross section of the sensors is shown in **Figure 1**. The top view shows the position of the sensor electrodes without the electrolyte coating. The cross-sectional view includes the electrolyte coating over the electrodes. There was no distinction observed between the electrolyte coating and pellet as the materials were of the same composition.

The microstructure and morphology of the electrolytes were analyzed using scanning electron microscopy (SEM) and Archimedes method. The electrochemical behavior of the sensors was characterized using a Gamry Reference 600 to perform impedance spectroscopy. Impedance measurements were performed for sensors operating over a temperature range of 600–700°C where the concentration of NO and NO$_2$ was varied from 0 to 100 ppm in O$_2$ concentrations of 1–18% with N$_2$ as the balance. Data were collected for dry and humidified (3–10% H$_2$O) environments using a standard gas handling system with mass flow controllers that maintained a flow rate of 100 standard cubic centimeters per minute (sccm). The Gamry instrument was configured to apply a signal amplitude of 50 mV over an operating frequency range of 1 Hz–1 MHz. Measurements were collected in triplicate to insure the data were consistent and stable. Equivalent circuit modeling using Gamry EIS300 software was used to acquire a detailed understanding of the electrochemical behavior of the sensors.
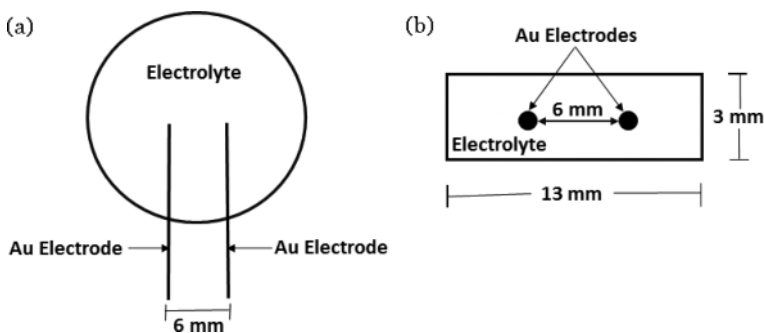


**Figure 1.** NO$_x$ sensor diagram: (a) top view, and (b) cross-sectional view with embedded Au wire electrodes.

## 3. Morphology and microstructure

The microstructure of the porous electrolyte can impact gas sensor reactions. Studies have found the porosity of the electrolyte effects gas transport to the triple phase boundary (TPB) [3, 7]. The TPB is the location where the electrolyte, electrode, and gas phase are in contact. The TPB is important as $NO_x$ sensing reactions take place along this boundary. Insufficient porosity within the electrolyte restricts gas transport to the TPB and limits sensor reactions. This usually results in a slow sensor response rate that is not practical for automotive applications. On the other hand, excess porosity allows gases to transport readily through the electrolyte, but also causes TPB reaction sites to become limited, which has the negative effect of decreasing $NO_x$ sensitivity. **Figure 2** shows typical SEM surface images for PSZ, FSZ, and PSZ–FSZ composite electrolytes. The particles composing the PSZ electrolytes (**Figure 2a**) were irregular in shape and varied from 0.1 to 0.3 μm in size; whereas, the FSZ electrolytes consisted of finer particles that seemed to be more uniform in size (largest diameter ~0.04 μm) and shape. The FSZ particle-to-particle connectivity, shown in **Figure 2b**, appeared to be greater than the particle connectivity between PSZ particles. The PSZ–FSZ composite electrolytes contained a well-distributed mixture of PSZ and FSZ particles, as shown in **Figure 2c**. In addition, larger pores were observed throughout the composite microstructure, in comparison to the single-phase electrolytes. **Figure 2d** shows an image of the microstructure of electrolytes containing PSZ coarse particles where the particle size ranged from about 0.4–1 μm. **Table 1** gives the porosity measurements for the various electrolytes that were determined via Archimedes method. The irregular shaped
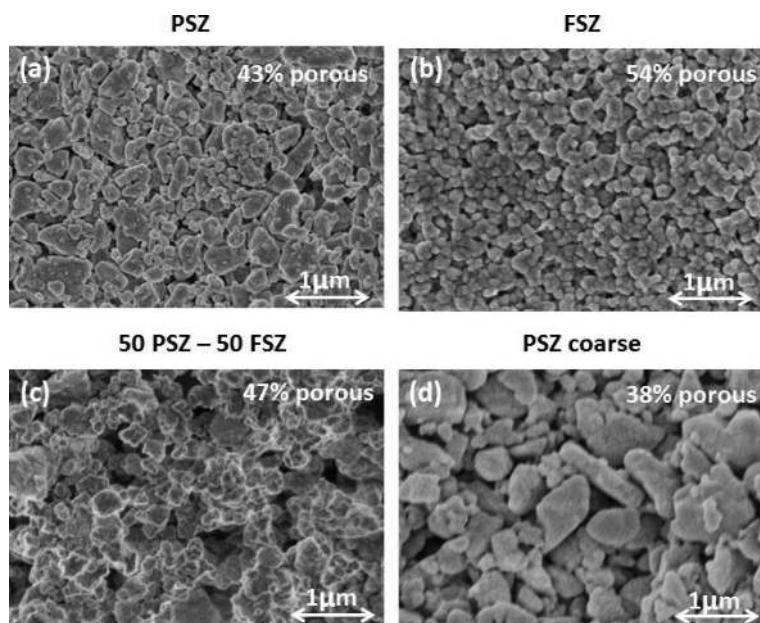


**Figure 2.**  SEM images of electrolytes composed of: (a) PSZ, (b) FSZ, (c) 50 PSZ–50 FSZ, and (d) PSZ coarse particles.

**Electrolyte porosity**

| PSZ | 75 PSZ–25 FSZ | 50 PSZ–50 FSZ | 25 PSZ–75 FSZ | FSZ | PSZ coarse |
| --- | --- | --- | --- | --- | --- |
| 43% | 45% | 47% | 50% | 54% | 38% |

**Table 1.** Electrolyte porosity based on Archimedes method.

PSZ particles allowed for closer packing of the particles, thereby, lowering the porosity of PSZ-based electrolytes.

## 4. Electrochemical response

Impedance spectroscopy is a powerful and commonly used technique for interpreting the electrical response of electrochemical devices and systems [8]. The impedance is an AC measurement that describes the opposition to current flow due to resistance, inductance, and capacitance effects. The impedance, $Z(\omega)$, varies with frequency, $f$, and is generally represented by the following equation:

$$Z(\omega) = Z' + jZ'' \tag{1}$$

where the angular frequency, $\omega = 2\pi f$. In addition, the real, $Z'$, and imaginary, $Z''$, impedance typically produce a semicircular shaped response or arc that is presented in the complex plane. In practice, more than one arc is common due to various reactions occurring at different rates. The impedance measurements for the NO$_x$ sensors in this work consisted of a high and low frequency arc. The high frequency arc (HFA) described electrochemical reactions occurring at the porous electrolyte; and, the low frequency arc (LFA) reflected electrode and interfacial reactions. **Figure 3** shows typical impedance data describing the electrochemical response of PSZ, FSZ, and 50 PSZ–50 FSZ-based sensors operating at 600°C with and without 100 ppm NO present under dry and humidified conditions. Data for sensors composed of PSZ coarse particles is included. For each type of sensor, the high frequency arc was independent of the gas concentration. In addition, the magnitude of the high frequency arc differed on account of the difference in ionic conductivity for PSZ (~0.08 S/cm) versus FSZ (~0.14 S/cm) [9]. The higher conductivity of FSZ contributed to the lower high frequency arc impedance. Thus, the magnitude of the high frequency arc decreased as the FSZ composition within the sensor increased. These observations were expected as the high frequency arc is known to depend upon the ionic conductivity and operating temperature of the electrolyte material [8]. In all cases here, the high frequency arc was incomplete on account of the high frequency limitation of the Gamry Reference 600 instrument. As the high frequency arc does not vary with gas concentration, it is generally not useful for interpreting the sensor response to NO$_x$ gas reactions. Therefore, acquiring a complete high frequency arc was not necessary for this study. For the low frequency arc, there was a decreased in magnitude when 100 ppm NO was added to the gas stream as shown in **Figure 3** for each sensor type. This change indicated electrode and interfacial reactions proceeded more readily when NO was present. The impedance data for sensors operating with 100 ppm NO$_2$ gas was
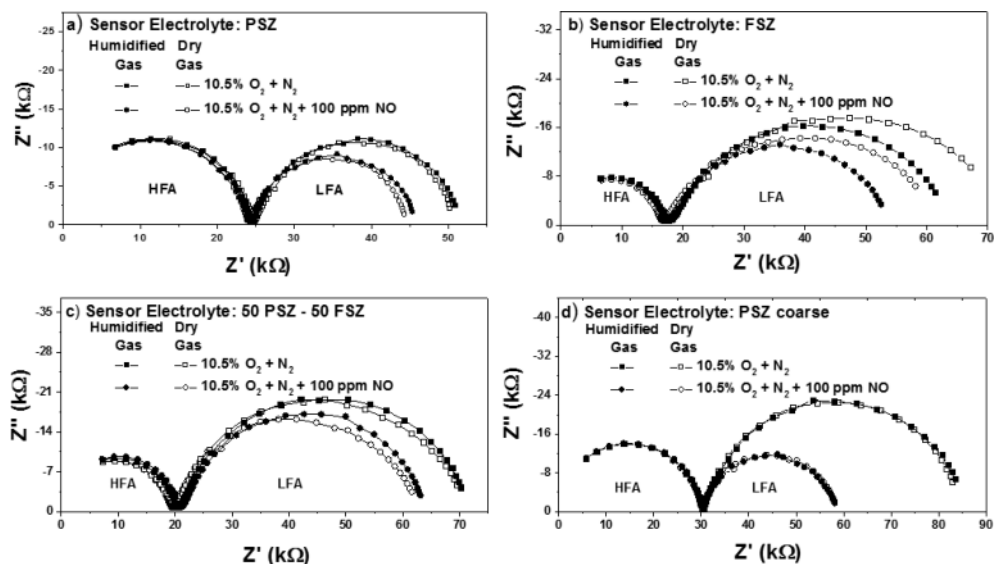
**Figure 3.** Impedance data collected at 600°C where the sensor electrolyte was: (a) PSZ, (b) 50 PSZ–50 FSZ, (c) FSZ, and (d) PSZ coarse under dry and humidified conditions.

very similar to that for NO. Thermodynamic conversion of $NO_2$ to NO takes place at elevated temperatures, such that at 600°C approximately 90% of $NO_2$ converts to NO. For this reason, data using NO gas is presented in this work.

The addition of water to the gas stream caused the low frequency impedance arc to slightly decrease for sensors with a PSZ, 75 PSZ–25 FSZ, and 50 PSZ–50 FSZ electrolyte. Quite the opposite behavior occurred for sensors containing a FSZ and 25 PSZ–75 FSZ electrolyte. The change in the impedance due to water cross-sensitivity is shown for sensors composed of PSZ, FSZ, and 50 PSZ–50 FSZ in **Figure 3a–c**. In other studies, analysis of water adsorption experiments at oxide surfaces have found that molecular water strongly adsorbs onto the surface of $Y_2O_3$ and surface reactions result in the formation of hydroxyl groups [10, 11]. Furthermore, computational studies indicate dissociation of water molecules is a mechanism for the formation of hydroxyl species at $Y_2O_3$–$ZrO_2$ surfaces; and, interfacial reactions between the oxide and hydroxyl groups can enhance oxygen ion conductivity [12]. However, it is also possible for adsorbed water molecules and hydroxyl species to block oxygen adsorption sites along the electrolyte/electrode interface and subsequently hinder interfacial reactions with oxygen [5]. In the present study, the $Y_2O_3$ content of the sensor electrolyte was approximately 4.7 and 8 mol% for PSZ and FSZ supported sensors, respectively. It is possible that the higher $Y_2O_3$ content of FSZ allowed greater adsorption of molecular water and hydroxyl groups to take place at sensors containing an FSZ based electrolyte, in comparison to sensors with ≥50 vol% PSZ. This would decrease the available sites for NO and $O_2$ adsorption. For such as case, triple-phase-boundary reactions requiring NO and $O_2$ would be limited, thereby, causing the sensor impedance to increase in the presence of water, as shown in **Figure 3b**. The slight decrease in impedance for PSZ sensors likely occurred due to enhanced oxygen ion conductivity. The lower $Y_2O_3$ content of

PSZ possibly resulted in less molecular water coverage such that sufficient adsorption of oxygen was able to take place. The adsorbed oxygen along with resulting hydroxyl species participated in reactions that produced oxygen ions, which enabled triple-phase-boundary reactions to more readily proceed at PSZ-based sensors.

As mentioned previously, the microstructure of the sensor electrolyte affects the number of particles and reaction sites along the triple-phase-boundary where NO$_x$ reactions take place. The SEM images in **Figure 2** indicate the sensor electrolyte microstructure differed for each sensor type. To determine the impact of the electrolyte microstructure on water cross-sensitivity, impedance measurements of sensors composed of coarse PSZ particles were collected. The impedance data indicated the electrochemical response for the sensors containing the course PSZ electrolyte particles did not significantly change when humidified gases were present, as shown if **Figure 3d**. Since similar behavior was observed for sensors composed of smaller PSZ particles it is unlikely that the microstructure of the electrolyte influenced the NO$_x$ sensor response during humidified gas conditions.

## 5. Equivalent circuit analysis

To further interpret the electrochemical response of the sensors equivalent circuit analysis was carried out. The impedance arcs in **Figure 3** were simulated using an equivalent circuit model consisting of resistors, R$_1$ and R$_2$, and constant phase elements, CPE$_1$ and CPE$_2$. **Figure 4** shows the equivalent circuit model that was used to analyze the impedance data for each of the sensors in greater depth. The components R$_1$ and CPE$_1$ described the resistance and nonideal capacitance behavior of the electrolyte. Components R$_2$ and CPE$_2$ corresponded to the interfacial resistance and nonideal capacitance behavior at the electrodes. The constants $n_1$ and $n_2$ describe the deviation from ideal capacitance behavior.

The behavior of R$_2$ and CPE$_2$ are useful for gaining insight about electrode reactions that influence sensing behavior. It was found that the interfacial resistance, R$_2$, decreased as the operating temperature of the sensor increase. This was expected as interfacial reactions, such as charge transfer, are able to proceed more readily at higher temperatures. The relationship between the capacitance, C, and constant phase element, CPE$_2$ is described by the following equation:

$$C = \frac{[(R_2)(CPE_2)]^{1/n}}{R_2} \tag{2}$$

where $n = 1$ describes the behavior of an ideal capacitor. Studies have reported that oxygen coverage at the electrode/electrolyte interface is described by the low frequency arc capacitance [13]. Oxygen accumulation at the electrode/electrolyte interface can hinder NO$_x$ transport to the interface and subsequently limit NO$_x$ sensing reactions. **Figure 5** shows the capacitance associated with sensors composed of PSZ, FSZ, and 50 PSZ–50 FSZ for dry, and humidified gas conditions. The capacitance for sensors with a PSZ electrolyte tended to be an order of magnitude greater than the capacitance of FSZ electrolyte sensors. It is possible that the difference in grain size between the PSZ and FSZ particles contributed to this difference in capacitance [14]. The capacitance of the 50
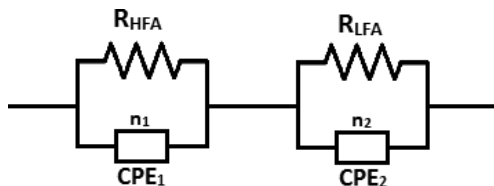
**Figure 4.** Equivalent circuit used to model the impedance data for PSZ, FSZ and composite PSZ–FSZ based sensors.
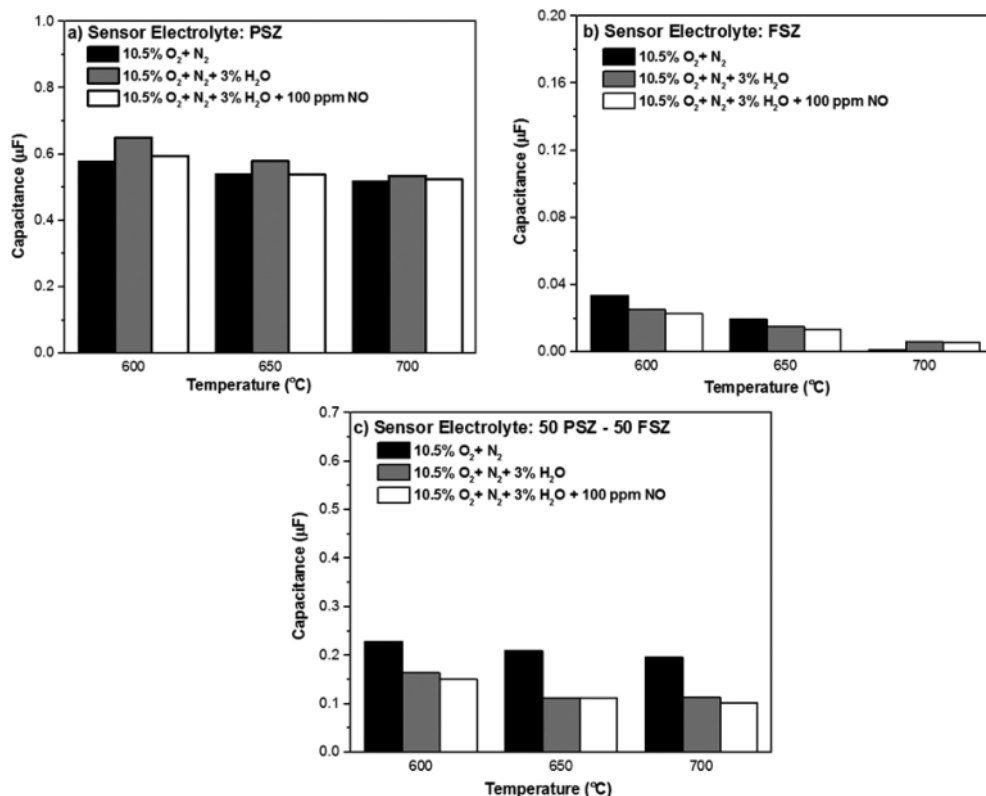


**Figure 5.** The capacitance of (a) PSZ, (b) FSZ and (c) 50 PSZ–50 FSZ based sensors with for dry and humidified gas conditions with respect to temperature.

PSZ–50 FSZ composite electrolyte sensors was about half of the capacitance calculated for the PSZ-based sensors. Adding 3% water to the gas stream caused a slight increase in the capacitance for the PSZ-based sensors; whereas, a decrease in the capacitance occurred for FSZ electrolyte sensors and especially the 50 PSZ–50 FSZ-based sensors. Adding additional water did not cause further changes in the capacitance. The addition of NO did not significantly alter the capacitance, which suggests NO molecules did not significantly impact oxygen coverage at the interface. The data in **Figure 5** also indicated a strong temperature dependence for capacitance of the FSZ-based sensors,

whereas, the PSZ and 50 PSZ–50 FSZ-based sensors displayed a less significant decrease in capacitance as the sensor-operating temperature increased. Overall, it appears the FSZ content in the composite electrolytes was beneficial for by limiting oxygen coverage at the interface such that water and NO molecules had greater opportunity to participate in triple-phase-boundary reactions. The PSZ component of the composite electrolyte helped to limited temperature dependence.

## 6. Sensor sensitivity

The angular phase component of the impedance, θ, is often more responsive the changes in NO$_x$ concentration, in comparison to other impedance parameters [1, 15]. For this reason, it is frequently used to evaluate NO$_x$ sensor sensitivity according to the following relationship:
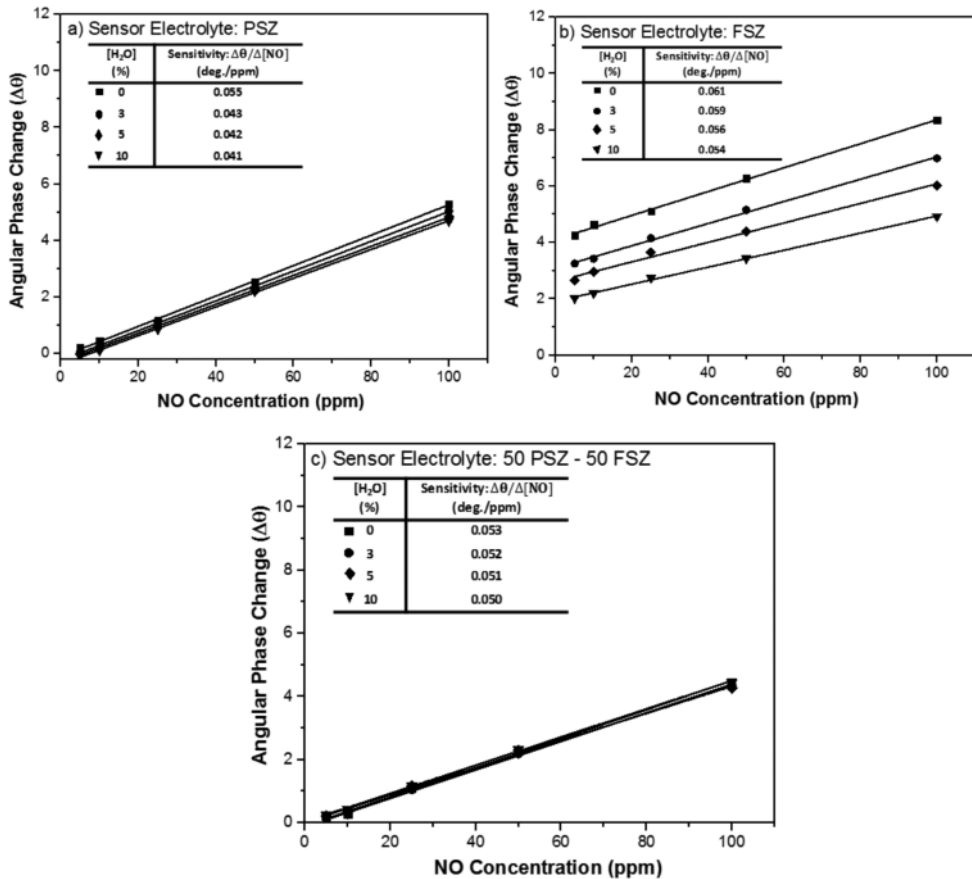


**Figure 6.** NO sensitivity for sensors with: (a) PSZ, (b) FSZ, and (c) 50 PSZ–50 FSZ electrolyte under dry and humidified gas conditions at 650°C.

$$\theta = arctan\left(\frac{Z''}{Z'}\right) \tag{3}$$

The change in the angular phase, $\Delta\theta$, is given by:

$$\Delta\theta = \theta_{O2} - \theta_{NO} \tag{4}$$

where $\theta_{O2}$ is the baseline response when 10.5% $O_2$ is present with $N_2$; and, $\theta_{NO}$ corresponds to the response when a specific amount of NO gas is added. **Figure 6** shows $\Delta\theta$ with respect to NO and water concentration for the PSZ, FSZ, and 50 PSZ–50 FSZ composite-based sensors at an operating frequency of 40 Hz at 650°C. Data was collected at 40 Hz as the maximum sensitivity was achieved at this operating frequency. The slope of the data, $\Delta\theta/\Delta[NO]$, is defined as the sensor sensitivity in units of degrees/ppm NO. The highest sensitivity was achieved during dry gas conditions for the various sensors. As the water concentration was increased in the gas
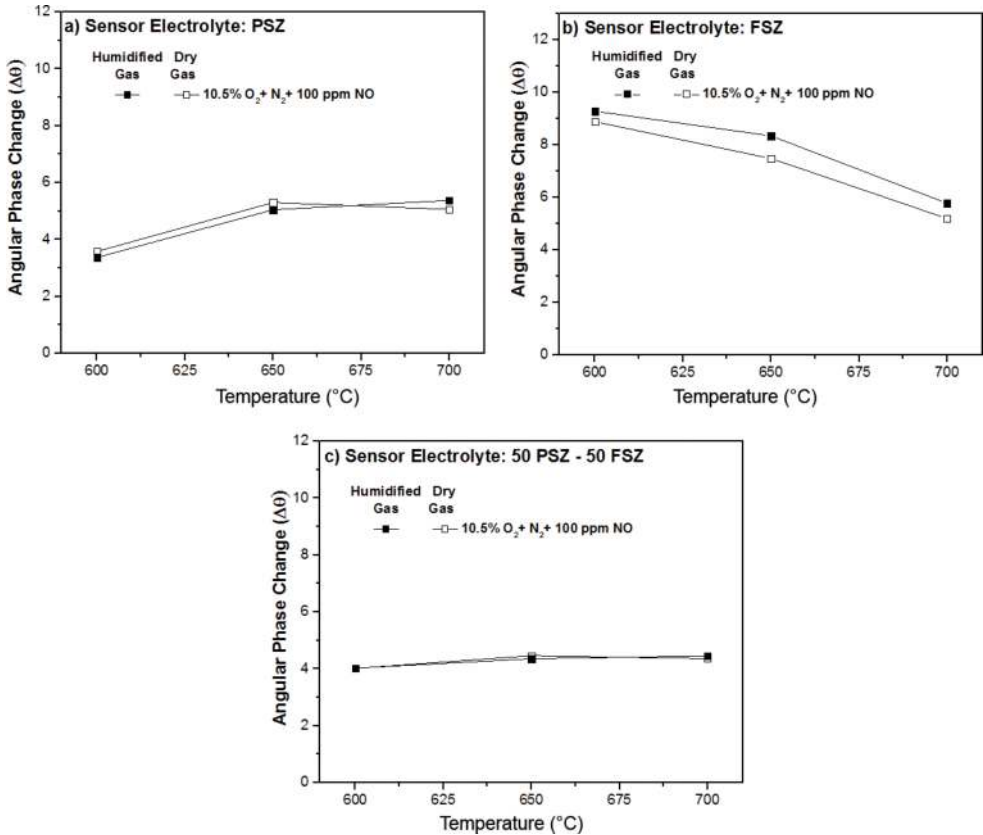


**Figure 7.** Change in angular phase response with respect to temperature for sensors composed of: (a) PSZ, (b) FSZ, and (c) 50 PSZ–50 FSZ electrolyte.

stream the sensitivity of the sensors decreased. However, the 50 PSZ–50 FSZ composite based sensors demonstrated the greatest tolerance to changes in the gas humidity as the sensitivity decreased very slightly. The sensors with an FSZ electrolyte had a higher sensitivity than sensors composed of PSZ, but the sensitivity of the FSZ based sensors decreased most significantly with increasing water in the gas stream. Although the FSZ electrolyte sensors provide higher sensitivity, the 50 PSZ–50 FSZ electrolyte contributes to a more reliable sensor.

In application the temperature of the sensor can fluctuate due to changes driving conditions. Thus, a stable NO$_x$ sensing response with respect to temperature is necessary in order to maintain accuracy. In the present study, the temperature dependence of the various sensors was observed by comparing Δθ with respect to the sensor-operating temperature, as shown in **Figure 7**. The sensing response of the FSZ-based sensors decreased with increasing operating temperature, as shown in **Figure 7b**. However, the PSZ and especially the 50 PSZ–50 FSZ based sensors were less dependent on temperature, as shown in **Figure 7a** and **c**. This data corresponded with the capacitance data presented in **Figure 5** where the capacitance of the sensors with an FSZ electrolyte also had a strong temperature dependence, in comparison to sensors with a PSZ and PSZ–FSZ electrolyte. Based on the data shown in **Figures 6** and **7**, sensors with the 50 PSZ–50 FSZ electrolyte were less prone to water cross-sensitivity and more tolerant to changes in the operating temperature.

## 7. Rate limiting mechanisms and activation energies

The gases traveling through the porous electrolyte and reacting at the triple-phase-boundary undergo various reaction steps including adsorption, dissociation, diffusion, charge transfer, and oxygen ion transport (not necessarily in that order). The porous microstructure creates specific pathways for gas and ionic transport. The electrolyte material and microstructure can impact how readily gas transport and related reactions occur. A common approach to interpreting rate-limiting mechanisms that impact gas transport and associated reactions is to evaluate the oxygen partial pressure (P$_{O2}$) dependence, which is described by the following power law relationship:

$$(P_{O2})^m \propto R_{LFA} \tag{5}$$

The power law exponent, $m$, is used to interpret specific rate-limiting mechanisms, and R$_{LFA}$ is the low frequency arc previously discussed. The P$_{O2}$ dependence of the PSZ, FSZ, and 50 PSZ–50 FSZ based sensors was determined by measuring the impedance response at oxygen concentrations ranging from 1 to 18% for dry and humidified gas conditions with and without NO. A plot of log(R$_{LFA}$) versus log(P$_{O2}$) was generated for the various gas conditions in order to determine the exponent $m$. **Table 2** provides the $m$ values determined for the sensors with a PSZ, FSZ, and 50 PSZ–50 FSZ electrolyte. Dissociative adsorption is the rate-limiting mechanism commonly associated with at P$_{O2}$ dependence where $m = 0.5$ [11, 16]. The data in the table indicated under dry gas conditions $m \approx -0.5$ for the PSZ-based sensors, which suggested dissociative adsorption was rate-limiting. Adding water to the gas stream without NO present decreased $m$ to $-0.43$ suggesting an additional rate-limiting mechanism, possibly charge transfer, became involved.

| | Power law exponent, m | | | |
| --- | --- | --- | --- | --- |
| | NO (ppm) | PSZ | 50 PSZ–50 FSZ | FSZ |
| Dry | 0 | −0.494 | −0.620 | −0.412 |
| Gas | 100 | −0.465 | −0.591 | −0.413 |
| Humidified | 0 | −0.427 | −0.626 | −0.471 |
| Gas | 100 | −0.512 | −0.553 | −0.472 |

**Table 2.** Power law exponent for sensors composed of the various electrolytes.

The charge transfer becomes a dominant rate-limiting step when $(P_{O2})^{-0.25} \propto R_{LFA}$. In the presence of NO and water, the PSZ-based sensors were apparently limited by dissociative adsorption as a $(P_{O2})^{-0.51}$ dependence was observed. A slightly lower $P_{O2}$ dependence was determined for the FSZ-based sensors. However, in the presence of both water and NO the dissociative adsorption seemed to be the dominant rate-limiting mechanism for FSZ-based sensors. Sensors with the composite 50 PSZ–50 FSZ electrolyte had a stronger $P_{O2}$ dependence, in comparison to the other sensors evaluated. The exponent, $m$ tended to be about −0.6, which suggested gas diffusion, may have participated as an additional rate-limiting mechanism. A $(P_{O2})^{-1}$ dependence has been associated with gas diffusion limitations. The porosity of the 50 PSZ–50 FSZ sensor was about 47%, which is expected to provide sufficient gas diffusion. However, it is possible that the composite microstructure resulted in tortuous pathways that interfered with gas diffusion. As a result the dissociative adsorption and gas diffusion could serve as rate-limiting mechanisms for sensors with a composite electrolyte.

The activation energy associated with the various sensors also aids interpretation of how readily sensor reactions are able to proceed. The activation energy, $E_a$, of the sensors for operating temperatures ranging from 600 to 700°C was determined using the Arrhenius equation the given below:

$$ln\left(\frac{1}{R_{LFA}}\right) = \left(\frac{E_a}{R}\right)\left(\frac{1}{T}\right) + ln(A_o) \qquad (6)$$

where $R_{LFA}$ is the diameter of the low frequency impedance arc, R represents the ideal gas constant, $T$ is temperature, and $A_o$ is the $y$-intercept. **Table 3** shows the activation energy

| | Activation energy (eV) | | | | | |
| --- | --- | --- | --- | --- | --- | --- |
| | NO (PPM) | PSZ | 75 PSZ–25 FSZ | 50 PSZ–50 FSZ | 25 PSZ–75 FSZ | FSZ |
| Dry | 0 | 1.067 | 1.119 | 1.148 | 1.150 | 1.230 |
| Gas | 100 | 1.017 | 1.101 | 1.122 | 1.125 | 1.205 |
| Humidified | 0 | 1.084 | 1.110 | 1.122 | 1.133 | 1.135 |
| Gas | 100 | 1.035 | 1.043 | 1.099 | 1.081 | 1.082 |

**Table 3.** Activation energy values for the various sensors.

calculated for each sensor type for dry and humidified conditions with and without NO present. The activation energy was the lowest for the single-phase PSZ-based sensors. The addition of water resulted in an increase in activation energy for the PSZ-based sensors and a decrease in the composite and FSZ-based sensors. Adding FSZ to the sensor electrolyte caused the activation energy to increase. This trend was observed for each of the various gas compositions measured and likely relates to the electrolyte microstructure. Other studies have reported that the activation energy in porous electrolyte NO$_x$ sensors tends to increase with increasing electrolyte porosity [3]. **Table 1** shows the porosity of the electrolytes increased as the FSZ content in the sensor electrolyte increased. The increase in porosity causes particle contact along the electrode/electrolyte interface to decrease resulting in fewer sites for reactions to take place, thereby, resulting in an increase in the activation energy.

## 8. Sensor response time and stability

Time-based measurements for the angular phase response, θ, were collected for sensors with a PSZ, FSZ, and composite PSZ–FSZ electrolyte. **Figure 8** shows the typical time-based response for sensors with a 50 PSZ–50 FSZ electrolyte as the NO composition was varied over 0–100 ppm. The dry and humidified data overlap as the 50 PSZ–50 FSZ electrolyte enables the sensor to be less prone to water cross-sensitivity. A baseline shift was observed for the time-based data collected for sensors composed the other electrolytes studied. The response time for each sensor was evaluated based on the $\tau_{90}$ response, which is the time required for the sensor to achieve 90%
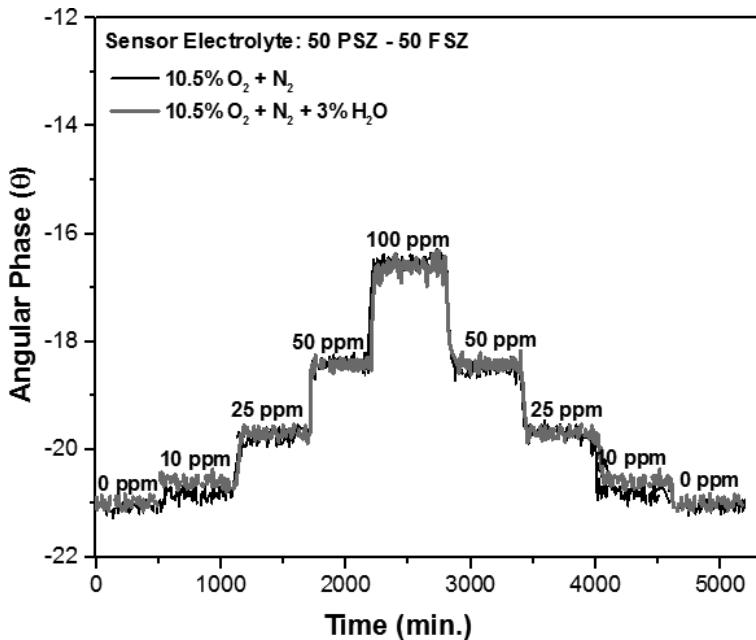


**Figure 8.** Angular phase response with respect to time for sensors composed of a 50 PSZ–50 FSZ electrolyte.

of the steady state response after a step change in gas concentration. **Table 4** shows the $\tau_{90}$ response for the various sensors. The sensors containing single-phase PSZ were the slowest as $\tau_{90} = 16$ s, which possibly relates to the lower ionic conductivity of the electrolyte, in comparison to single-phase FSZ-based sensors where $\tau_{90} = 5$ s. As seen in **Table 4**, the sensor response time decreased resulting in a faster sensor as the FSZ concentration increased.

The stability of a 50 PSZ–50 FSZ based sensors was evaluated for over 150 hours at 650°C and an operating frequency of 40 Hz with 3% water present. **Figure 9** shows sensor drift was negligible for both the baseline response where θ remained about −17.25°, and the sensor response with humidified gas where θ remained nearly constant at about −16.25°. This data suggests that the 50 PSZ–50 FSZ electrolyte is capable of providing a very stable sensing response. Further evaluation is necessary to determine the extent of the 50 PSZ–50 FSZ based sensor stability over longer time intervals.

| Sensor electrolyte | Time constant – $\tau_{90}$ (s) | | | | |
| --- | --- | --- | --- | --- | --- |
| | PSZ | 75 PSZ–25 FSZ | 50 PSZ–50 FSZ | 25 PSZ–75 FSZ | FSZ |
| Dry gas | 16 | 14 | 10 | 7 | 5 |
| Humidified gas | 14 | 12 | 11 | 5 | 4 |

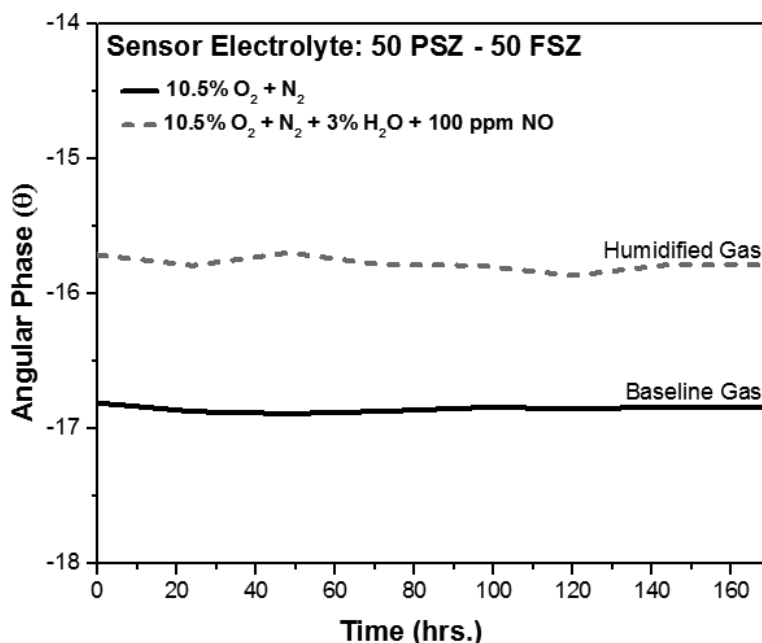**Table 4.** The $\tau_{90}$ response of the sensors composed of the various electrolytes.



**Figure 9.** Stability of a 50 PSZ–50 FSZ sensor over several hours of operation.

## 9. Conclusions

Impedance spectroscopy was used to interpret the electrochemical response of NO$_x$ sensors composed of PSZ, FSZ, and PSZ–FSZ composite electrolytes during operation under dry and humidified gas conditions. Analysis of the electrochemical response of the 50 PSZ–50 FSZ based sensors indicated PSZ contributed to lower water cross-sensitivity, while FSZ promoted NO$_x$ sensitivity. It was also determined that the electrolyte microstructure influenced sensor sensitivity, but did not impact water cross-sensitivity. Dissociative adsorption was considered to be the dominant rate-limiting mechanism for each of the sensors. Adding water to the gas stream did not appear to significantly alter the rate-limiting mechanism. The response of the FSZ-based sensors was strongly depended upon the operating temperature, whereas the response of sensors containing PSZ, and particularly the 50 PSZ–50 FSZ, was less dependent on temperature. The response time of the sensors decreased as the concentration of FSZ increased within the sensor electrolyte indicating the FSZ contributed to a rapid sensor response rate. Overall, sensors composed of the 50 PSZ–50 FSZ composite electrolyte demonstrated significant sensitivity to NO and low cross-sensitivity to water with negligible temperature dependence.

## Acknowledgements

## Author details

Erica Perry Murray*, Khawlah Kharashi and Kehinde Adedeji

*Address all correspondence to: emurray@latech.edu

Louisiana Tech University, Ruston, Louisiana, USA

## References

[1] Martin LP, Woo LY, Glass RS. Impedancemetric NO$_x$ sensing using YSZ electrolyte and YSZ/Cr$_2$O$_3$ composite electrodes. Journal of the Electrochemical Society. 2007;**154**:J97–J104. DOI: 10.1149/1.2430646

[2] Woo LY, Glass RS, Novak RF, Visser JH. Diesel engine dynamometer testing of impedancemetric NO$_x$ sensors. Sensors and Actuators B: Chemical. 2011;**157**:115–121. DOI: 10.1016/j.snb.2011.03.034

[3]  Cui L, Han F, Dai W, Murray EP. Influence of microstructure on the sensing behavior of $NO_x$ exhaust gas sensors. Journal of the Electrochemical Society. 2014;**161**:B34–B38. DOI: 10.1149/2.019403jes

[4]  Soltis RE, Ding Y, Visser JH, Kubinski DJ. Influence of $H_2O$ on $NO_x$ sensors. ECS Transactions. 2006;**10**:173–178. DOI: 10.1149/1.2357257

[5]  Sakai N, Yamaji K, Horita T, Xiong YP, Kishimoto H, Brito ME, Yokokawa H. Erratum to effect of water on electrochemical oxygen reduction at the interface between fluorite-type oxide-ion conductors and various types of electrodes. Solid State Ionics. 2005;**176**:2327–2333. DOI: 10.1016/j.ssi.2005.08.002

[6]  Kharashi K, Murray EP. Effect of $Al_2O_3$ in porous zirconia electrolytes for NO sensing. Journal of the Electrochemical Society. 2016;**163**:B633–B637. DOI: 10.1149/2.0761613jes

[7]  Steil MC, Thevenot F, Kleitz M. Densification of Yttria-Stabilized Zirconia Impedance Spectroscopy Analysis. Journal of the Electrochemical Society.1997;**144**:390–398. DOI: 10.1149/1.1837416

[8]  MacDonald JR, Barsoukov E. Impedance Spectroscopy: Theory, Experiment and Applications. 2nd ed. New York: Wiley; 2005. DOI: 10.1002/0471716243

[9]  Zhang C, Li C, Zhang Z, Ning X, Liao H, Coddet C. Ionic conductivity and its temperature dependence of atmospheric plasma-sprayed Yttria stabilized zirconia electrolyte. Materials Science and Engineering B. 2007;**137**:24–30. DOI: 10.1021/1a9917031

[10]  Kuroda Y, Hamano H. Mori T, Yoshikawa Y, Nagao Y. Specific adsorption behavior of water on a $Y_2O_3$ surface. Langmuir. 2000;**16**:6937–6947. DOI: 10.1016/j.mseb.2006.10.005

[11]  Raz S, Sasaki K, Maier J, Riess I. Characterization of adsorbed water layers on $Y_2O_3$-doped $ZrO_2$. Solid State Ionics. 2001;**143**:181–204. DOI: 10.11016/S0167-2738(01)00826-8

[12]  Chaopradith DT, Scanlon DO, Catlow RA. Adsorption of water on Yttria-stabilized zirconia. The Journal of Physical Chemistry C. 2015;**19**:22526–22533. DOI: 10.1021/acs.jpcc.5b06825

[13]  Woo L, Martin LP, Glass RS, Wensheng W, Sukwon J, Gorte RJ, Murray EP, Novak RF, Visser JH. Effect of electrode composition and microstructure on impedancemetric nitric oxide sensors based on YSZ electrolyte. Journal of the Electrochemical Society. 2008;**155**:J32–J40. DOI: 10.1149/1.2804766

[14]  Guo X, Maier J. Grain boundary blocking effect in zirconia: a Schottky barrier analysis. Journal of the Electrochemical Society. 2001;**148**:E121–E126. DOI: 10.1149/1.1348267

[15]  Orazem M, Tribollet B. Electrochemical Impedance Spectroscopy. Hoboken: Wiley; 2008. DOI: 978-0-470-04140-6

[16]  Van Herle J. McEvoy A. Thampi KR. Oxygen reduction at porous and dense cathodes for solid oxide fuel cells. Conductivity Measurements Electrochemica Acta. 1994;**29**:1675–1680.